Fundamental Study Of Arcing Behavior In Boundary Layer Of MHD Generator

Author(s): I. Inoue, M. Ishikawa, and J. Umoto

Session Name: Generators C

SEAM: 28 (1990)

SEAM EDX URL: https://edx.netl.doe.gov/dataset/seam-28

EDX Paper ID: 1443

FUNDAMENTAL STUDY OF ARCING BEHAVIOR IN BOUNDARY LAYER OF MHD GENERATOR

Isao Inoue
Yatsushiro National College of Technology
Hirayama-shinmachi Yatsushiro, Kumamoto, 866, JAPAN

Motoo Ishikawa and Juro Umoto
Department of Electrical Engineering, Kyoto University
Yoshida-honmachi, Sakyoku, Kyoto, 606, JAPAN

Abstract

This paper deals with the two-dimensional time-dependent numerical simulations to make a comparative investigation of experimental results on Faraday type MHD electrical power generators. The current streamline function is used to decrease the number of unknown variables and to easily obtain values of the electric and fluid quantities. The arcing behaviors, the arc characteristics and the current distributions in the channel can be studied with the help of streamline function obtained by applying the Finite Element Method. The comparison of the experimental results with calculated results is based on the electrode voltage drop. It is found that these numerical simulations agree very well with the experimental results on the anode side.

That is, at the coal-fired MHD channel, the slag sticking to the surface of the electrode wall plays the role of a thermal insulating material and it results that the current flow becomes the diffuse discharge with a locally concentrated current in the slag layer. At the petroleum-fired MHD channel, the current flow becomes the big arc discharge in the boundary layer at a low temperature of the electrode wall.

The numerical calculations show that the arcing behaviors and the arc characteristics which have periodicity. The arcs are held on the electrode wall with a width, and are made the narrow concentrated current(narrow arc discharge) on the electrode wall. The phenomena depends on the wall temperature and the load resistance.

1. Introduction

Faraday type MHD electrical power generators have many segmented electrodes which are divided into many parts along the flow direction in order to prevent a short circuit of the Hall electric field. Because the electrodes are usually cooled with flowing water, there is thermal boundary layer in the MHD channel. This gives that the electrical conductivity of the gas near the electrode is expressed as a strong function of the electrode wall temperature. The electrical conductivity of the gas in the boundary layer is small compared to the one in the core region.

The arcs generated in the boundary layer can be much different depending on the MHD channel being coal-fired or petroleum-fired.

At the coal-fired MHD channel, because the slag layer along the electrode functions as an insulating material and because the electrical conductivity of the slag layer is of a comparatively large value, the current flow tends to become the diffuse discharge in the slag layer and results in an arc discharge with a constant and locally stable structure on the electrode in the boundary layer. On the other hand, at the petroleum-fired MHD channel with a low temperature electrode, the electrical conductivity of the gas near the electrode is very small compared to that of the core region. The current flow, hence, concentrates at a point near the electrode and becomes an arc discharge in the boundary layer which keeps the negative characteristics.

The arcs generated in the bundary layer depend strongly upon the surface temperature of the electrode wall and the electrode materials.

There are various kinds of the arcs, from a micro arc to a big arc.

There have been many studies about constricted currents or arc discharges in view of the detailed experimental results and of the theoretical investigation[1-8]. A large number of experimental results were examined from the view point of arc characteritics and one method was proposed for the arc's analysis[9], and the study[10] of the arc characteristics was made by considering the division of the boundary layer into three physical regions. Several papers[11,12] have reported on simulations in which arcs move on the electrode in the boundary layer.

The arcing behaviors are, however, found experimentally to be a very complicated phenomenon with a variety of arc types mixed in the boundary layer, so there are still many aspects which must be clarified about the arcing behavior and the arc characteristics. The simulation for the arcing behavior near the electrode appropriates to the fundamental analysis of the arc characteristics. With two-dimensional time-dependent numerical simulation for the actual MHD generator[13], we made a comparative investigation[14] of the experimental results, the current flow distributions for the various temperatures of the electrode wall and the arcing behaviors.

In this paper, by the same two-dimensional simulation, we make a comparative investigation of the current flow mechanism near the electrode wall for coal-fired and of the arcing behaviors and the arc characteristics in the boundary layer for petroleum-fired, where the electrode temperature is changed.

2. Theoretical Model

Basic Equation

The basic equations are the Maxwell equations and the generalized Ohm's law for electrodynamics as follows:

$$\nabla \cdot \mathbf{J} = 0 \tag{1}$$

$$\nabla \times \mathbf{E} = 0 \tag{2}$$

$$\mathbf{J} = \sigma(\mathbf{E} + \mathbf{u} \times \mathbf{B}) - (\beta / B)(\mathbf{J} \times \mathbf{B}) \tag{3}$$

where $\mathbf{J}$ is the current density, $\mathbf{E}$ the electric field, $\mathbf{u}$ is the gas velocity, $\mathbf{B}$ is the applied magnetic flux density, and σ and β are the electrical conductivity of the gas and Hall parameter, respectively.

The gas temperature is governed by the following law of energy conservation:

$$\rho C_p\left(\frac{\partial T}{\partial t} + \mathbf{u} \cdot \nabla T\right) = \kappa_e \nabla^2 T + \frac{J^2}{\sigma} + \mathbf{u} \cdot (\mathbf{J} \times \mathbf{B}) \tag{4}$$

where ρ is the total mass density, C_p is the specific heat at constant pressure, T is the gas temperature, κ_e is the effective thermal conductivity, respectively.

In the boundary layer, the sharp temperature gradient will be produced by the local Joule heating. The velocity distribution is given independently.

Assumptions and Initial Conditions

Figure 1 shows the cordinate system and channel geometry used in the calculations.

All quantities are assumed to be constant in the direction of the magnetic field(z direction) and calculations are made in the plane(x-y plane) perpendicular to the z direction.

The anode and the cathode are assumed to have the same electrical nature ; i.e. the cathodic condition is not taken into account.

The depth of the slag layer sticking on the electrode depends on a temperature of the electrode wall and becomes as following equation.

$$\delta_{sl} = 3.65 \cdot 10^{-3} - 2.092 \cdot 10^{-6} \cdot T_w \quad (T_w \leq 1745\text{K}) \tag{5}$$

Equation (5) was obtained by the experimental results[15].

The gas velocity and the magnetic flux density assumed to have the form $\mathbf{u} = (u, 0, 0)$ and $\mathbf{B} = (0, 0, B)$ in which $\mathbf{u}$ is constant in time and $\mathbf{B}$ in space and time.

The laminar sublayer region is assumed to exist on the electrode walls in the boundary layer.

The distributions of the initial gas temperature T and the gas velocity u are as follows:

In the core region, T and u are constant.

In the boundary layer region, the values of T and u are calculated by using the (1/7)-th power law. In the laminar sublayer region, they are proportional to the distance from wall.

The effective thermal conductivity is calculated as follows :

In the core region, the values of the effective thermal conductivity are constants. In the boundary layer region, they are calculated with a Prandtl's mixing-length model by

$$\kappa_e = (\kappa \rho l^2 / \mu)(\partial u / \partial y) \tag{6}$$

where κ is the thermal conductivity, l the mixing length, μ the viscosity, y the distance from electrode wall, respectively.

In the laminar sublayer region, they are assumed to be thermal conductivity κ.

The electrical conductivity σ, Hall parameter β for the gas and the electrical conductivity σ_s for the slag are given by the following equations.

$$\sigma = 89.9 \cdot P_s^{-0.51} \cdot T^{1.855} \cdot \exp(-2.52 \cdot 10^4 / T) \tag{7}$$

$$\beta = 4.43 \cdot B \cdot P_s^{-0.99} \cdot T^{0.97} \tag{8}$$

$$\sigma_s = 7.7 \cdot 10^5 \cdot \exp(-1.9376 \cdot 10^4 / T) \tag{9}$$

where P_s is the static pressure.

Current Streamline Function

In analyzing near-wall phenomena, the current streamline function Ψ defined by equation (10) is applied in order to decrease the unknown variable numbers.

$$J_x = \frac{I_L}{W}\left(\frac{\partial \Psi}{\partial y}\right), \qquad J_y = -\frac{I_L}{W}\left(\frac{\partial \Psi}{\partial x}\right) \tag{10}$$

where I_L is the load current and W the channel width. Using the above assumptions, Eq.(3) is reduced to the following set:

$$\left.\begin{aligned} E_x &= (J_x - \beta J_y)/\sigma \\ E_y &= (-\beta J_x + J_y)/\sigma + uB \end{aligned}\right\} \tag{11}$$

An equation for Ψ is obtained by substituting Eqs.(10) and (11) into Eq.(2) as

$$\frac{\partial}{\partial x}\left[\frac{1}{\sigma}\frac{\partial \Psi}{\partial x} + \frac{\beta}{\sigma}\frac{\partial \Psi}{\partial y}\right] - \frac{\partial}{\partial y}\left[\frac{\beta}{\sigma}\frac{\partial \Psi}{\partial x} - \frac{1}{\sigma}\frac{\partial \Psi}{\partial y}\right] = 0 \tag{12}$$

In order to solve Eq.(12), the boundary conditions have to be specified over the perimeter of the calculation plane, which is shown in Fig.1.

The calculations are made in one segment region (AEHD). The boundary condition on the electrode (BC and FG) is $E_x = 0$ and Eqs.(10), (11) becomes

$$\beta\left(\frac{\partial \Psi}{\partial x}\right) - \left(\frac{\partial \Psi}{\partial y}\right) = 0 \quad \text{(on BC and FG)} \tag{13}$$

On the insulators, $J_y = 0$ is assumed and then Ψ = constant is obtained on AB, CD, EF and GH with equation (10). Then, the value of Ψ is taken equal to zero on the left insulator (AB and EF), as follows

$$\Psi = 0 \quad \text{(on AB and EF)} \tag{14}$$

The integration of J_y over the electrode gives the load current I_L,

$$I_L = -W\int_B^C J_y\,dx \tag{15}$$

Substituting Eq.(10) into Eq.(15) yields

$$I_L = -W\int_B^C \frac{I_L}{W}\frac{\partial \Psi}{\partial x}\,dx = I_L\,[\Psi(C)-\Psi(B)] \tag{16}$$

By considering Eqs.(14) and (16), the value of Ψ must be unity on the right insulator, namely

$$\Psi = 1 \quad \text{(on CD and GH)} \tag{17}$$

Since periodicity is assumed over the one segment, the boundary condition on DH and AE is given as,

$$\Psi\,\text{(on DH)} - \Psi\,\text{(on AE)} = 1 \tag{18}$$

Since each electrode is connected to a external load R_L as shown in Fig.1, the load current is obtained by integrating Eq.(11) and substituting Eq.(10) into that as follows:

$$I_L = \int_0^h uB\,dy \Big/ \left[R_L + \frac{1}{W}\int_0^h \frac{1}{\sigma}\left(\frac{\partial \Psi}{\partial x} + \beta\frac{\partial \Psi}{\partial y}\right)_{x=s/2} dy\right] \tag{19}$$

where h is the channel height and s the one pitch length. Here it is obvious that the first term of the dominator of the right-hand side of Eq.(19) corresponds to an internal resistance of the plasma.

Gas Temperature

By the assumption of two-dimensionality, the law of energy conservation (4) is reduced to as follows:

$$\rho C_p\left[\frac{\partial T}{\partial t} + u\frac{\partial T}{\partial x}\right] = \kappa\left[\frac{\partial}{\partial x}\frac{\partial T}{\partial x} + \frac{\partial}{\partial y}\frac{\partial T}{\partial y}\right] + \frac{J_x^2 + J_y^2}{\sigma} + uBJ_y \tag{20}$$

The boundary conditions for the gas temperature T is given as:

$$T = T_w = \text{constant} \quad \text{(on AD and EH)} \tag{21}$$

$$T\ \text{(on AE)} = T\ \text{(on DH)} \tag{22}$$

where T_w is the electrode wall temperature.

In the core region, the gas temperature is assumed to have the constant value, which means that the gastemperature in the boundary layer region changes to equation (20).

3. Results and Discussions

Numerical procedure

The partial differential equations (12) and (20) for Ψ and T, respectively, are solved iteratively by the Finite Element Method using bilinear rectangular elements. Even meshes are employed in x direction (divided into 24) and uneven meshes in y direction (46-58). The time step (dt) is selected to satisfy the stability condition.

Geometrical and gasdynamic Conditions

In order to compare the numerical results with the experimental ones, the dimensions of the channel used in the calculations have been chosen equal to that of the ETL-Mark Ⅶ B-channel: channel height h=240[mm], channel width W=75[mm] one electrode pitch lengths=24[mm] and electrode width C=20[mm].

The gasdynamic conditions are also chosen to have almost the same value as the experimental ones: gas core temperature T = 2,500[K], magnetic flux density B = 2.5[T], gas velocity u = 800[m], static pressure P_s=1[atm], boundary layer width δ = 30[mm], laminar sublayer width δ_s = 1.0[mm] and thermal conductivity is 1.5[W/mK] in the core region.

Arcing behaviors and arc characteristics at coal-fired MHD channel

In our calculations, the slag layer is assumed to be in the solid state and depth of the slag layer to be 0.72[mm] by Eq.(5).

Figure 3 shows the time-dependent variation of the current streamline and the temperature distributions near the electrode at wall temperature of 1400[K] and load resistance of 4.0[Ω].

As shown in Figures, the current stream-line distributions represent the deflection in the slag layer. An uniform current streamline flows into a large part of the electrode and a concentrated current streamline is recognized on a part of it. It takes 34.5 milli seconds for a part of the slag surface to be melted by the joule heating at the anode side. Figures 3-1 (b) and 3-1' show the current streamline distributions after melting of a part of the slag surface.

The concentrations of the current streamline are seen on the up-stream and down-stream edges of the electcode in the slag layer and the laminar sublayer, and in these layers, the current streamline is disturbed.

Figure 3-2 shows the temperature distribution at 150 milli second in the slag and boundary layers. In this figure, the temperature is 2340 [K] at the point A, the current density is 9.3 [A/cm^2] at point B and the electrode voltage drop is about 45 Volts at the anode side.

Melting of the slag surface spreads wholly on the gas side, but at the inside of the slag layer there is no melting of the slag. The arc generates locally in the area between the slag surface and turbulent boundary layer, and the concentration of the current streamline occured locally in the slag layer reaches the electrode.

We explan above as follows.

Because the slag layer along the electrode functions as thermal insulating material, a large quantity of heat carried from the core region through the turbulant boundary is accumulates in the laminar sublayer, whereas a small quantity of heat is transferred to the slag layer.

With time, the heat accumulated in the laminar sublayer increases the temperature of a part of the slag surface so that the current flow is partially concentrated in the slag layer and that part of the slag surface is melted. The place which melts is not an insulating material yet, is changed into gas and has a large electrical conductivity, which results in a change in the current streamline in the laminar sublayer.

The current is, moreover, variated by spreading the part of the melted slag surface by the heat accumulated in the laminar sublayer. By the repetition of the above process, the amount of the current concentrated becomes the arc discharge with high temperature and large current density in the laminar sublayer.

At the steady state, the current flow is the arc discharge with a constant and locally stable structure in the boundary layer. In the slag layer, the current flow is the diffuse discharge which consists of a lot of uniform current and a local concentration of current with high density.

Since the concentrated current reaches the electrode with high density, the arc spot appears on the electrode.

It was reported on the experimental result[10] which indicate that the current is concentrated on one point of the electrode with the slag layer in many electrode conditions.

The results of these numerical calculation are similar to the experimental phenomenon.

<u>Arcing behaviors and arc characteristics at petroleum-fired MHD channel</u>

In experiments, the current density was about 1.5[A/cm²] in the channel of the MHD generator and the arcs were generated as points on the electrode. Similar phenomena are calculated as shown.

For $t<0$, the current density is set to about 1.5[A/cm²] and the arc spot is produced on the electrode. For $t>0$, the electrical and fluid quantities are calculated in the channel. Here and hereafters, t denotes time.

Figure 4 dipicts the time-dependent variation of the current streamline and the temperature distributions in the boundary layer at wall temperature of 500[K] and load resistance of 5.0 [Ω]. As shown in the diagrams, an arc appears just at the up-stream edge of the electrode,. then moves to the down-stream edge of the electrode and disappears soon after. At the same time, a new arc generates at the up-stream edge, and the same process repeats. The anodic arc cycle (generate-move-disappear-generate) is about 470 micro seconds, whereas the cathodic arc cycle about 230 micro seconds including hold-time(about 40 micro seconds) at the down-stream edge.

The anodic arc cycle is longer compared to the cathodic cycle. This is due to the Hall effect.

The above process depends on a balance between the Hall effect, the effect of convection and the breaking force driven by the Lorentz force.

Since the three-dimensional effect and the interaction of gas velocity and electrical quantities are neglected in the calculation, the arc cycle becomes relativily short compared with the real situation.

In this calculation, the electrode voltage drop on the anode is about 95 volts at the current density J_y=-1.24[A/cm²]. The experimental result is about 75 Volts at the same current density, so the calculated voltage result is about 20% higher than the experimental result.

With reference to Figure 4-2 and the other calculated data, the temperature of the arcs on the anode side is about 2240-2460[K], whereas that on the cathode is about 2350-2570[K] and the current density of the arcs on the anode is about 17.1-23.1[A/cm²], that on the cathode is about 25.4-30.0[A/cm²].

This shows that the arcs generated in the boundary layer grow into the big arcs with high temperature and large current density in itself under the condition of the wall temperature of 500[K].

Figure 5 shows the time-dependent variation of the current streamline and the temperature distributions in the boundary layer at wall temperature of 800[K] and load resistance of 2.0[Ω]

As shown in the diagrams, on the anode side, the arc appears on the up-stream side of the electrode, and then moves to the down-stream side along the gas flow. The arc is held on the electrode at about two thirds of the electrode length. At this time, two arcs are in existence in the boundary layer. One of the arcs is held already on the electrode, the other is generating newly on the up-stream side of the electrode.

The position is about a quarter of the electrode length from the up-stream edge of the electrode. The arc held on the electrode transfers its energy to a newly generating arc, becomes smaller and smaller and eventually disappears.

The new arc moves down-stream on the electrode and is held on the electrode, then moves to the up-stream side where it is held, then moves to the down-stream side where it is further held, and the same process repeats.

Finally, the arc becomes fixed at about one thirds of the electrode length from the up-stream edge with a width of 2-3[mm] on the electrode.

On the other hand, on the cathode side, an arc appears just at the up-stream edge of the electrode, then moves to the down-stream edge of the electrode and disappears after it is held for about 100 micro seconds. At the same time, a new arc generates at the up-stream edge, then moves and disappears, and the same process repeats. The cathodic arc cycle is about 160 micro seconds.

The voltage drop on the anode side is about 88 Volts, wheras that of experimental results is about 86 Volts.

This shows that the calculated result agrees very well with those observed.

From Figure 5-2 and the other calculated data, the temperature of the arcs on the anode side is about 2400-2560[K], whereas that on the cathode is about 2480-2650[K]. The current density of the arcs on the anode is about 11.0-14.9[A/cm²], whereas that on the cathode is about 11.4-40.2 [A/cm²]. The above mentioned represent the big arc discharge phenomenon.

This simulation represents the big arc discharge fixed on the electrode with a width of 2-3[mm] at the wall temperature of 800[K].

The reason why the big arc is fixed on the electrode, is explained as follows.

While the arc is moving down-stream on the electrode, the effect of convection is decreased gradually by the influence of the wall temperature and the thermal conduction, the arc is then kept on the down-stream of the electrode by equilibrium between the effect of convection, the Hall effect and the Lorentz force. Since the effect of convection is more decreased from the same reason, the arc moves to the up-strem side of the electrode by a stronger action of the Hall effect. Then, because the temperature gradient of the arc becomes larger and larger during the movement of the arc to the up-stream side, the arc stops at the up-stream due to the equilibrium, and its position becomes down-stream behind the last position. With large temperature gradient, the arc moves to the down-stream side on the electrode by the effect of convection, and the same process repeats.

Finally, the arc is held on the electrode with a width by the balance between the Hall effect, the Lorentz force and the effect of convection.

Figure 6 dipicts the time-dependent variation of the current streamline and the temperature distributions in the boundary layer at the wall temperature of 1200[K] and load resistance of 2.0 [Ω]. As shown in the diagrams, on the anode, an arc appears on the up-stream side of the electrode, then moves down-stream along the gas flow, and is held on a half position ($X=S/2$) of the electrode length, not arriving at the down-stream edge of the electrode. At this time, there are two arcs; one is held at half electrode length to have the decreased current density, and the other is generated newly on the up-stream side of the electrode. The arc held on the electrode transfers its energy to a newly generating arc, becomes smaller and smaller, and eventually disappears. The position of the arc generated on the up-stream side of the electrode is about one thirds of the electrode length from the up-stream edge. The arc generated is held for about 80 micro seconds. During this time, it's temperature and current density increase. The arc then grows into the big arc with high temperature and large current density, moves to the down-stream side, is held, and disappears at half position of the electrode length, and the same process repeats. The anodic arc cycle is about 420 micro seconds.

On the other hand, on the cathode, only one arc generates on the up-stream side of the electrode, then moves to the down-stream side and is held on the down-stream edge of the electrode.

After one process, the arc is held steadily on that position with high temperature and large current density in itself.

The electrode voltage drop on the anode is about 70 volts, whereas that of experimental results is about 75 volts. The above result shows that there is a close relation between experimental and calculated results.

With reference to figure 6-2 and the other calculated data, the temperature of the arc on the anode is about 2470-2630[K], whereas that on the cathode is about 2860-2870[K]. The current density of the arc on the anode is about 14.1-32.1[A/cm^2], whereas that on the cathode is about 40.1-41.2[A/cm^2]. That indicates the big arc discharge phenomenon.

The results obtained by the same simulation for changing the load resistance are in agreement with the above mentioned results without the positions and times of the arc cycle.

Because the anode arc cycle, 420 micro seconds is a very short time compared to the order of a second, the arc can be assumed with a narrow current concentration (narrow arc discharge) to have about 2.5[mm] width on the electrode.

This simulation, therefore, represents the narrow arc discharge phenomenon with high temperature and large arc current density.

The reason the positions of the anode arc change repeatedly from about one thirds of the electrode length to about a half length on the electrode, is explained as follows.

When the arc held on the up-stream side of the electrode has a large temperature gradient, the arc begins to move to the down-stream side on the electrode, depending on a balance of the Hall effect, the effect of convection and the Lorentz force.

While the arc is moving to the down-stream on the electrode, the temperature gradient of the arc is gradually relaxed by the influence of the wall temperature and the thermal conduction.

Therefore, by weakening the effect of convection, the arc is held on the electrode by the equiliblium of the effect of convection, the Hall effect and the Lorentz force.

For the same reason, the temperature gradient of the arc is further relaxed at that place held on the electrode and the Hall effect acts more strongly. The result is that the arc held on the electrode disappears little by little and a new arc is generated on the up-stream side of the electrode. Because the convection still has an albeit, small effect the new arc, the position of the arc generated on the electrode still depends on a balance of the Hall effect, the effect of convection and the Lorentz force at the time. The arc grows to a big arc which has high temperature and large current density, and moves to the down-stream side on the electrode in the boundary layer.

4. Conclusions

There are various kinds of the arc in MHD channels and the arc discharge phenomena are essentially three-dimensional in real situations so that it is rather complicated to fully analyze its mechanism.

The present two-dimensional numerical model, however, can simulate some experimental results for the arcing behavior:

(1) At a coal-fired MHD channel, the slag layer along the electrode wall functions as a thermal insulating material.

The current flow becomes the arc discharge, in the boundary layer, which has a constant and locally stable structure with high temperature, while in the slag layer, the current flow becomes the diffuse discharge which consists of a lot of uniform current and a locally concentrated current with a large current density.

(2) At a petroleum-fired MHD channel, on the anode side, the calculated results of the electrode voltage drop agree very well with those observed, demonstrating that there is a close relation between experimental and culculated results.

At a low temperature of the electrode wall, the current flows become the big arc discharge with high temperature and large current density.

The generation, movement, holding and disappearance of the arc depend on a balance between the Hall effect, the effect of convection and the breaking force driven by the Lorentz force.

The positions of the generated arc on the electrode and the behavior of cyclic arc are dicided mainly by the effect of convection and by the electrode temperature.

These simulations can be show the arcing behaviors and the arc characteristics. The arcs have a periodicity in the boundary layer, and the arcs are held on the electrode wall with a width and the arcs are composed of a narrow big arc discharge on the electrode wall. The phenomena depends on the temperature of the electrode wall and the load resistance.

Acknowledgements

Computer were carried out with Super Computer in Data Processing Center, Kyoto University.

References

1. D.A.Oliver, "A Constricted Discharge in Magnetohydrodynamic Plasma", 15th Symp. on Eng. Asp. of MHD, Paper, 1976.
2. R.Hernberg, et al., "Boundary Layer Breakdown and Discharge on Cold Cathode in Alkali-Seeded Plasma", 8th Int. Conf. on MHD Elec. Power Generation, Vol.I, 1983, pp.231.
3. G.Zankl, et al., "Results of The IPP Test Generator and The Design of A 10 MWel Short-Time Combuster MHD Generator", 14th Symp. on Eng. Asp. of MHD, 1974, pp.I.1.1.
4. N.Kayukawa, et al., "SFC-Type MHD Generator Performance", 9th Int. Conf. on MHD Elec. Power Generation, Vol. II, 1986, pp.449.
5. R.Nelson, et al., "Transient Phenomena in Coal-Fired MHD Generators:Electrical Effect of Slag in a Diffuse-Mode Magetohydrodynamic Generators", Research Project 468-3 Final Report, Stanford University, High Temperature Gas Dynamics Laboratory, 1882
6. Cott, et al., "Slag Behavior in MHD Generators :Physical Phenomena and Engineering Consequences", 26th Symp. on Eng. Asp. of MHD 1988
7. E.Schmitt, et al., "Resent Investigations of Cathode Wall Nonuniformities", 10th Int. Conf. on MHD Elec. Power Generation, 1989, pp.V.34.
8. B.Gupta, et al., "Electrothermal Instabilities in MHD Boundary Layers", 10th Int. Conf. on MHD Elec. Power Generation, 1989, pp.V.114.
9. R.J.Rosa, "Boundary Layer Arc Behavior:Theory and Experiment", 9th Int. Conf. on MHD Elec. Power Generation, Vol. II, 1986, pp.637.
10. I.Sadovnik, et al., "Electrode Arcing Phenomena in MHD Generators", 19th Symp. on Eng. Asp. of MHD, 1981, pp.10.1.1.
11. M.Ishikawa, et al., "Interaction Between Electrodynamics and Gas Dynamics near Electrodes of MHD Generator", 10th Int. Conf. on MHD Elec. Power Generation, 1989, pp.V.74.
12. T.Hara, et al., "Streamer Development in Noble Gas MHD Channels in Relation to Seed Fractions", 20th Symp. on Eng. Asp. of MHD, 1982, pp.10.7.1.
13. Y.Kusaka, et al., "Experiments of ETL Mark VII MHD Facility", 8th Int. Conf. on MHD Elec. Power Generation, Vol.I, 1983, pp.B.1.
14. I.Inoue, et al., "Arcing Behavior in Boundary Layer of MHD Generator", 10th Int. Conf. on MHD Elec. Power Generation, 1989, pp.V.61.
15. M.Rodgers, "Fluid Mechanics and Thermal Behavior of MHD Channel Slag Layer", 17th Symp. on Eng. Asp. of MHD, 1979, pp.c.2.1.

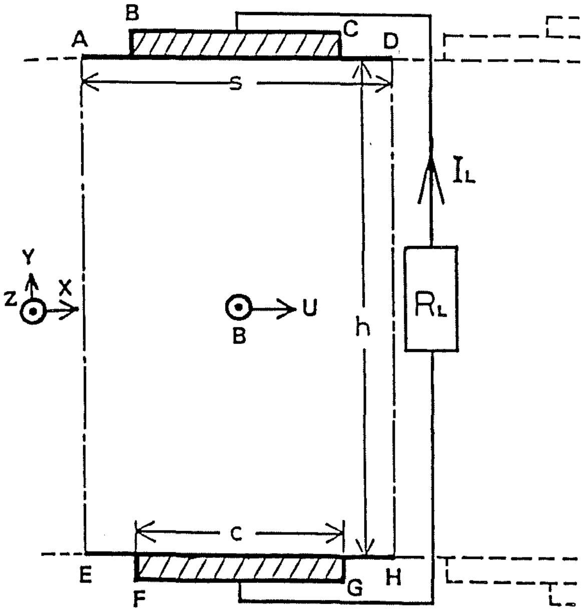

Fig.1 Schematic diagram of Faraday type MHD generator and coordinate system.

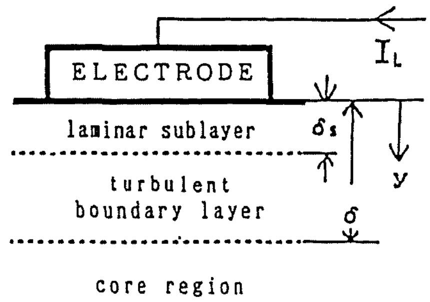

Fig.2 Near electrode wall

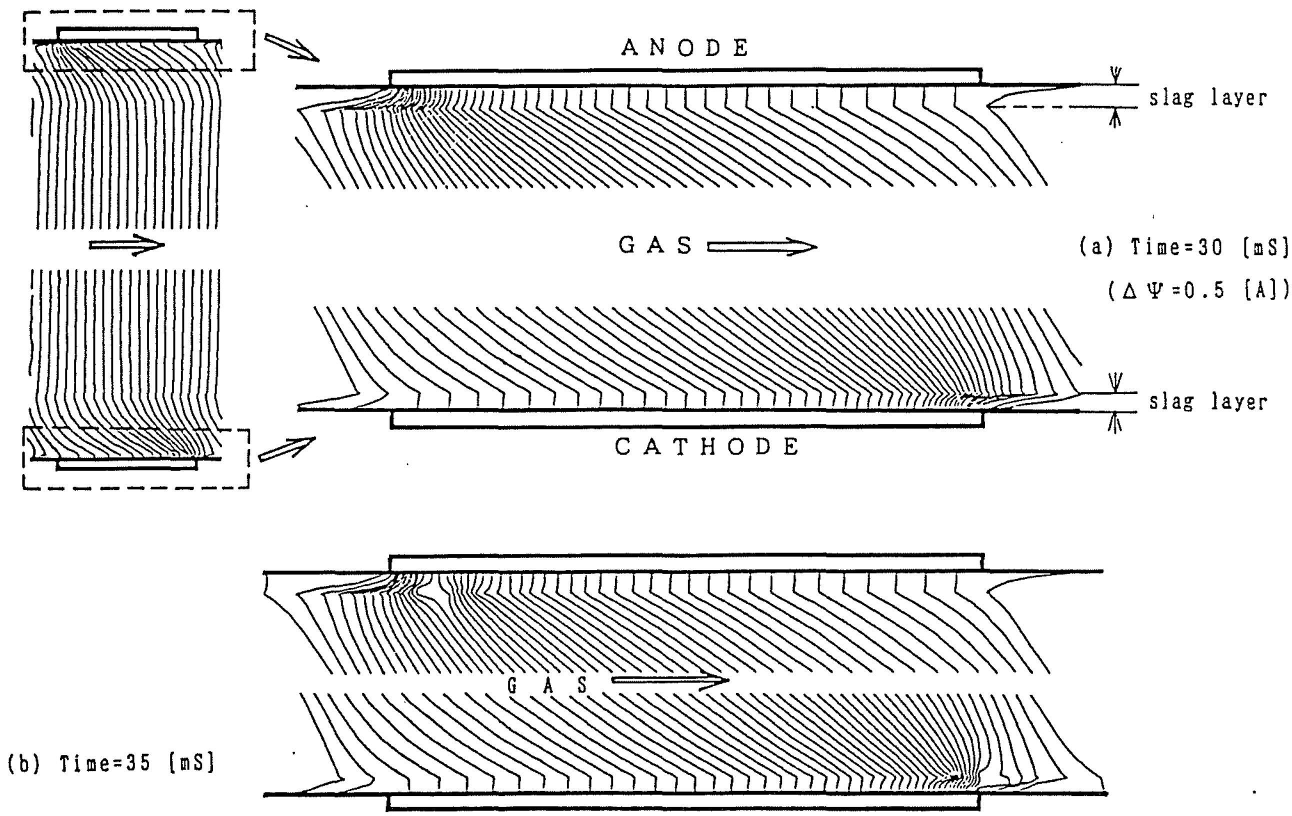

Fig.3-1 Time-dependent current streamline distributions in the slag and boundary layers at coal-fired MHD channel for wall temperature=1400[K], load resistance=4.0[Ω]

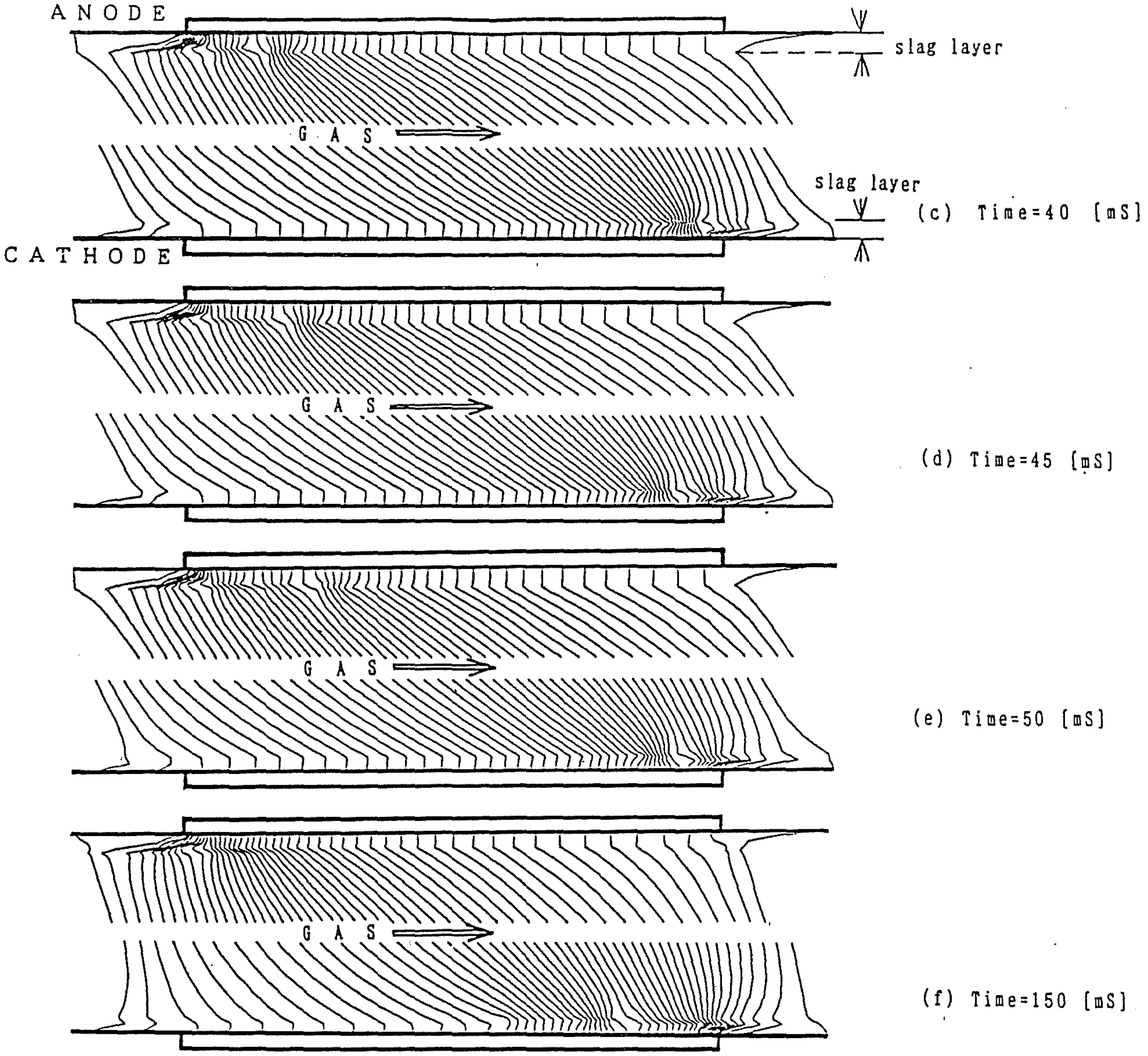

Fig.3-1' Time-dependent current streamline distributions in the slag and boundary layers at coal-fired MHD channel for wall temperature=1400[K], load resistance=4.0[Ω]

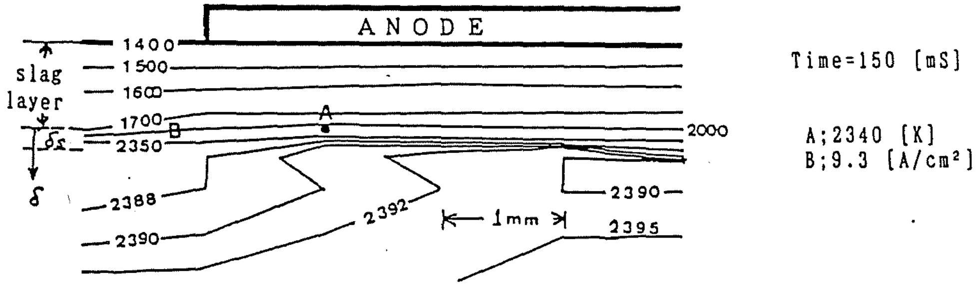

Fig.3-2 Time-dependent temperature distribution in the slag and boundary layers at coal-fired MHD channel for wall temperature=1400[K], load resistance=4.0[Ω].

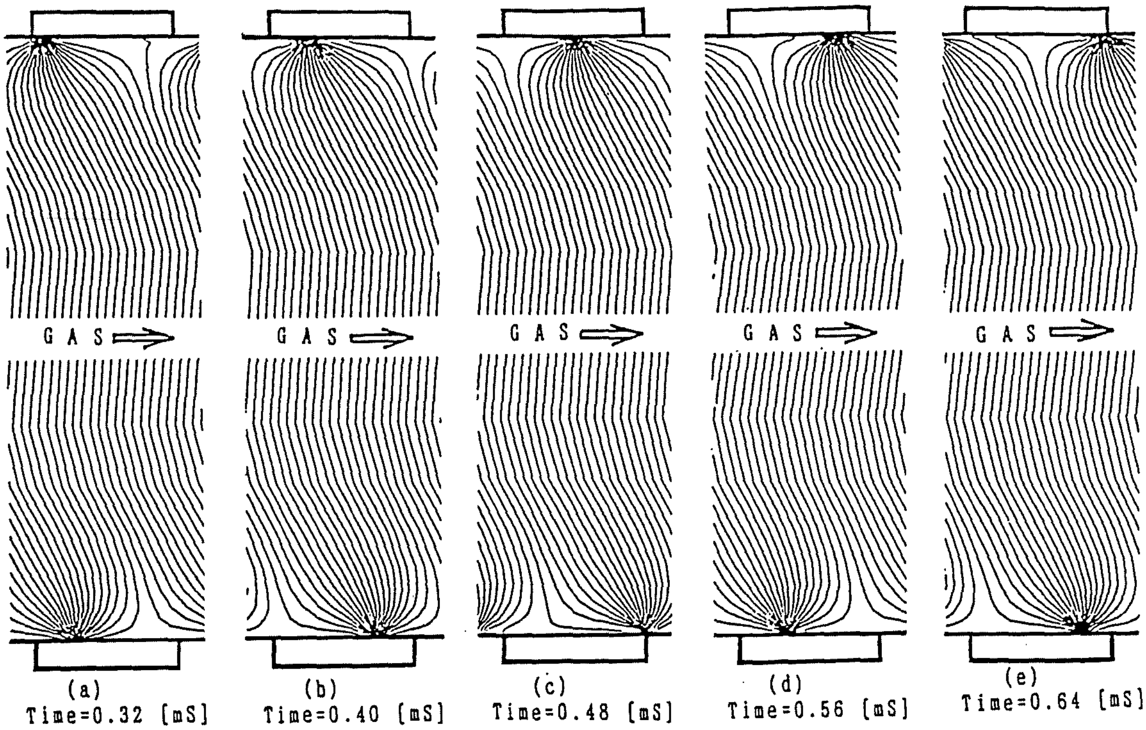

Fig.4-1 Time-dependent current streamline distributions in the boundary layer at petroleum-fired MHD channel for wall temperature=500[K], load resistance=5.0[Ω].

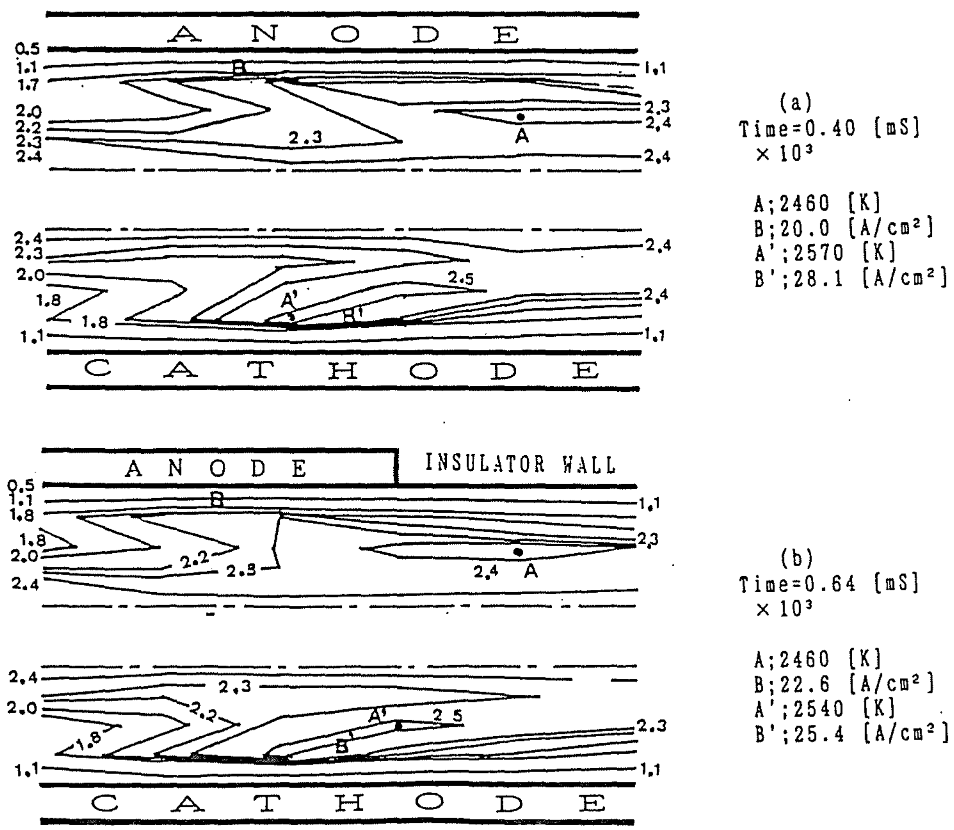

Fig.4-2 Time-dependent temperature distributions in the laminar sublayer at petroleum-fired MHD channel for wall temperature=500[K], load resistance=5.0[Ω].

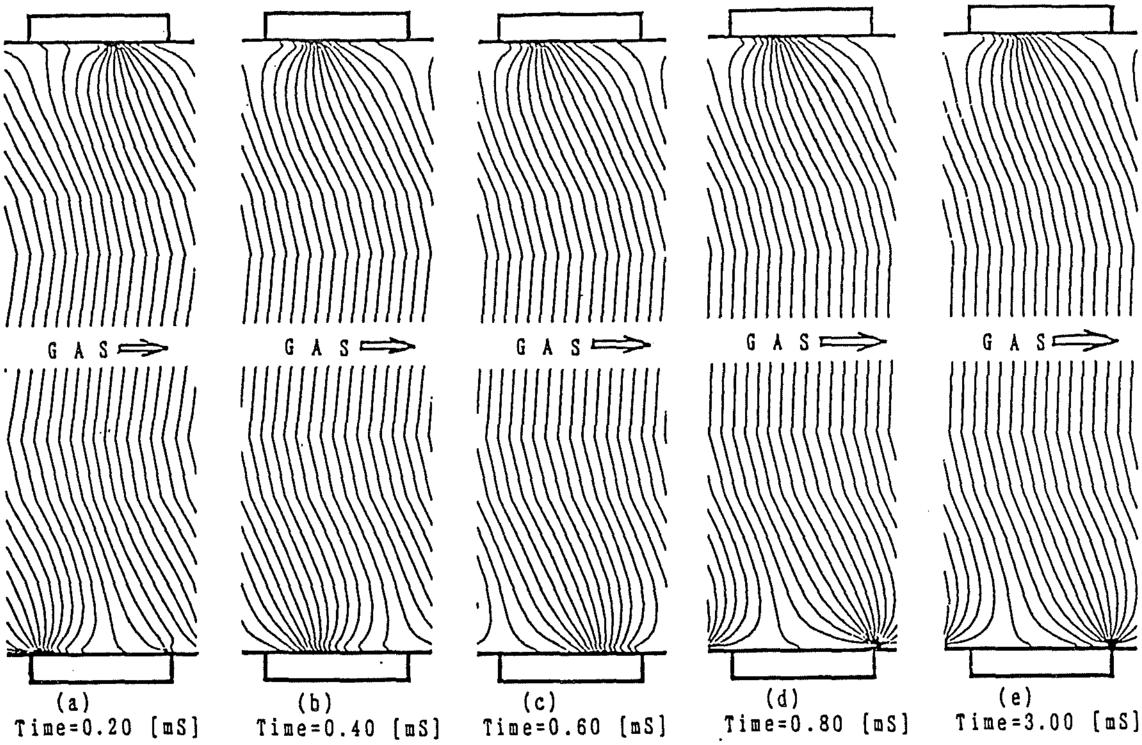

Fig.5-1 Time-dependent current streamline distributions in the boundary layer at petroleum-fired MHD channel for wall temperature=800[K], load resistance=2.0[Ω].

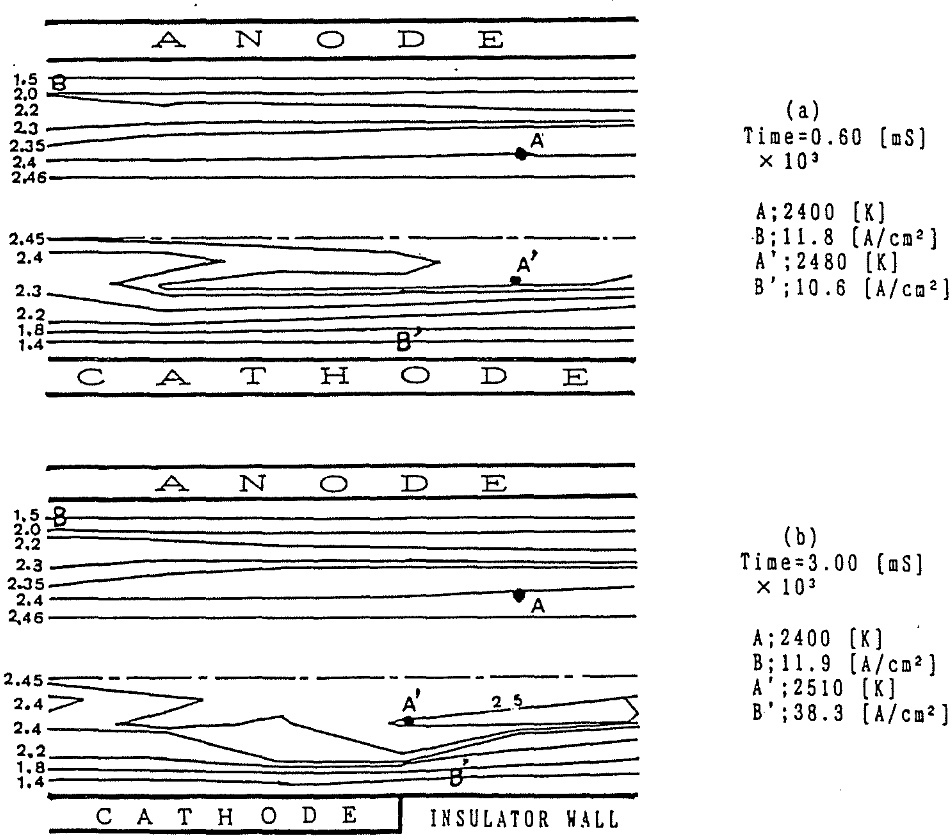

Fig.5-2 Time-dependent temperature distributions in the laminar sublayer at petroleum-fired MHD channel for wall temperature=800[K], load resistance=2.0[Ω].

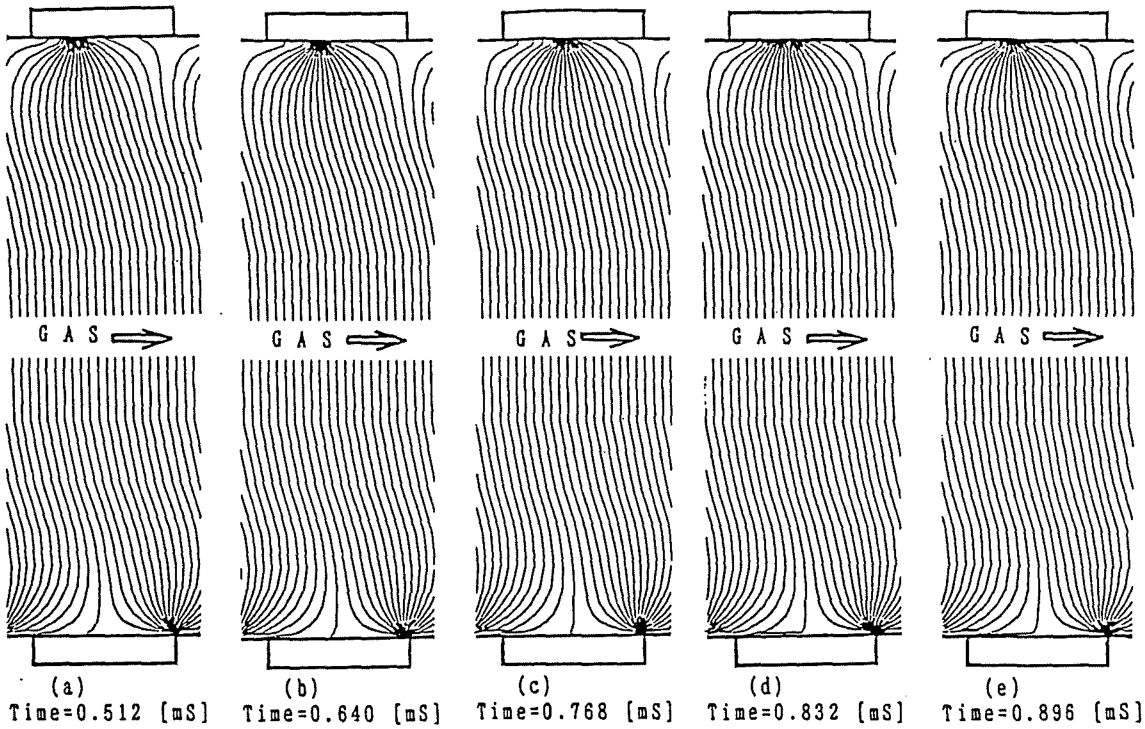

Fig.6-1 Time-dependent current streamline distributions in the boundary layer at petroleum-fired MHD channel for wall temperature=1200[K], load resistance=2.0[Ω].

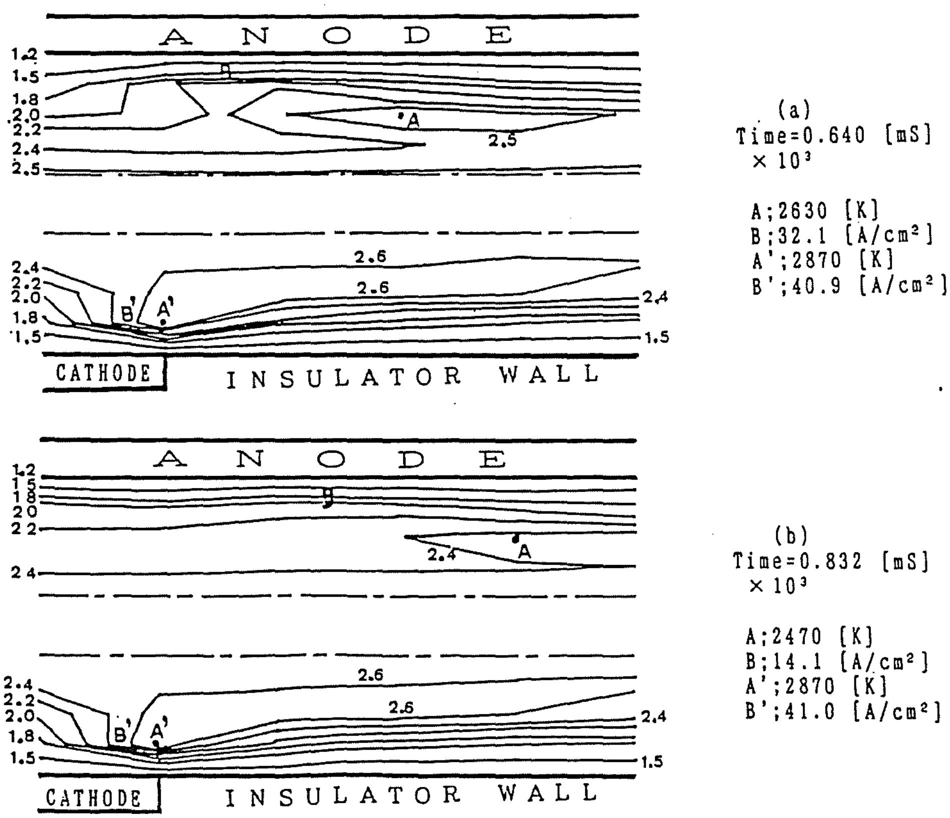

Fig.6-2 Time-dependent temperature distributions in the laminar sublayer at petroleum-fired MHD channel for wall temperature=1200[K], load resistance=2.0[Ω].